PONTIFICIA UNIVERSIDAD CATOLICA DE CHILE
ESCUELA DE INGENIERIA

A TECHNIQUE FOR RECONSTRUCTION USING INTENSITY ORDER (TRIO): AN APPLICATION TO UNDERSAMPLED DATA

LEONARDO ANDRÉS RAMÍREZ MAC-LEAN

Thesis submitted to the Office of Research and Graduate Studies
in partial fulfillment of the requirements for the degree of
Master of Science in Engineering

Advisor:
PABLO IRARRÁZAVAL M.

Santiago de Chile, August 2008

PONTIFICIA UNIVERSIDAD CATOLICA DE CHILE
ESCUELA DE INGENIERIA

A TECHNIQUE FOR RECONSTRUCTION USING INTENSITY ORDER (TRIO): AN APPLICATION TO UNDERSAMPLED DATA

LEONARDO ANDRÉS RAMÍREZ MAC-LEAN

Members of the Committee:
PABLO IRARRÁZAVAL M.
MARCELO GUARINI H.
CARLOS LIZAMA Y.
GONZALO CORTÁZAR S.

Thesis submitted to the Office of Research and Graduate Studies
in partial fulfillment of the requirements for the degree of
Master of Science in Engineering

Santiago de Chile, August 2008

A mis padres, Soledad y Pedro

ACKNOWLEDGMENTS

It is very difficult for me to write the acknowledgments, there are so many people I would like to give thanks to and I do not want to forget about anyone. The fact that this is the last thing I write for this thesis does not make it any easier, as emotions overwhelm me by knowing I am about to finish this work and probably close a chapter in my life.

I will start by thanking my advisor Pablo Irarrázaval, he has guided me throughout this process and his help has been invaluable. I have learned many things from him in the scientific area, but I specially value his passion for research and his honesty and guidance in not scientific matters. I also thank Marcelo Guarini, who has always been available for guidance and support and has always been concerned about the wellbeing of my family.

During the development of this research, I have had the pleasure of working with a great group of people. I have to start thanking Claudia Prieto who is responsible for convincing me to start my research in this area as well as allowing me to finish it. Her help has made this thesis possible and her friendship has given me strength throughout my work. I have to thank Cristián Tejos next. He is someone who astonishes me, he is always doing a million different things and even so he has always been available to help me with a smile on his face. With Francisco Prieto, Marcelo Andía, Ignacio Vallejos and Carlos Sing-Long I have had the most interesting talks. We have discussed about scientific issues, politics, philosophy and life among other things, but their humor is priceless. I think there has never been a day in which I have not had at least a couple of laughs with them. The latest arrival was Esther Guiu, who was able to cheer me up when I needed it most and give me the energy I needed to complete this work. I can not thank her enough.

I have left the most important for last: my parents. Their love and support throughout the years is what makes possible anything I do. Even though we are currently living over 11743 kilometers apart, I have always felt their continuous support.

TABLE OF CONTENTS

LIST OF FIGURES

LIST OF TABLES

ABSTRACT

The non invasive nature of Magnetic Resonance Imaging (MRI) combined with its flexibility have made it a popular medical imaging technique. However, long acquisition times have limited its use for 3D and dynamic images. One approach used to overcome this problem has been to undersample the k-space, allowing shorter acquisition times, followed by a reconstruction algorithm that recovers the non-acquired data employing some sort of prior information. Most reconstruction methods such as keyhole, sliding window and k-t BLAST are prone to introduce spatial or temporal blurring. We propose to use the information that allows to sort the pixels of an image from brightest to darkest as the additional information. This order information can be obtained from low resolution images, adjacent slices in 3D imaging or from prior reconstructions. The technique for reconstruction using intensity order (TRIO) finds the images by minimizing the discrepancy between the acquired and reconstructed data, subject to the intensity order constraints. The proposed method was used to reconstruct 2D dynamic cardiac images using the temporal average image to provide the initial order information. TRIO was also applied as a second stage reconstruction using first keyhole, sliding window or k-t BLAST to estimate the order information. In all cases TRIO achieved reconstructions with less spatial and temporal blurring as well as less structured error than the first reconstructions.

Keywords: MRI, Undersampling, Reconstruction, Order.

RESUMEN

La naturaleza no invasiva de las Imágenes de Resonancia Magnética (MRI por sus siglas en inglés) junto con su flexibilidad las han convertido en una técnica de imágenes médicas muy usada. Sin embargo, los largos tiempos de adquisición han limitado su uso para imágenes dinámicas y 3D. Una forma de resolver este problema ha sido el submuestreo del espacio-k, permitiendo menores tiempos de adquisición, seguido por un algoritmo de reconstrucción que recupera la información que no fue adquirida usando algún tipo de información previa. La mayoría de los métodos de reconstrucción tales como keyhole, sliding window y k-t BLAST son susceptibles a introducir borrosidad espacial o temporal en las imágenes. Proponemos usar la información que permite ordenar los píxeles de una imagen desde el más brillante al más oscuro como información previa. Esta información de orden se puede obtener de imágenes de baja resolución, de un corte contiguo en imágenes 3D o de reconstrucciones previas. Esta técnica de reconstrucción usando el orden de las intensidades (TRIO por sus siglas en inglés) encuentra las imágenes mediante la minimización de la discrepancia entre los datos adquiridos y reconstruidos, sujeto a las restricciones dadas por el orden de intensidades. El método propuesto fue usado para reconstruir una secuencia dinámica 2D de imágenes cardiacas usando el promedio temporal como fuente inicial de la información de orden. TRIO también fue aplicado como una segunda etapa de reconstrucción usando inicialmente keyhole, sliding window y k-t BLAST para estimar la información de orden. En todos los casos, TRIO logró reconstrucciones con menos borrosidad espacial y temporal así como un error menos estructurado que las primeras reconstrucciones.

Palabras Claves: MRI, Submuestreo, Reconstrucción, Orden.

1. GENERAL INTRODUCTION

1.1. MRI Basics

Magnetic resonance imaging (MRI) is a technique which allows to produce internal images of an object based on its physical or chemical characteristics. MRI is based on the nuclear magnetic resonance (NMR) phenomenon which was independently demonstrated by Felix Bloch (Bloch, 1946) and Edward Purcell (Purcell et al., 1946) in 1946. Atoms with an odd number of protons and/or an odd number of neutrons posses a nuclear spin angular momentum. This atoms are simply referred to as spins and act as small magnetic dipoles. It was not until 1973 when Paul Lauterbur (Lauterbur, 1973) obtained the first MRI by spatially encoding the NMR signals and not until 1980 when MRI was introduced to the medical field. The most common element detected by MRI Scanners is the single proton Hydrogen (^{1}H) which is present in water throughout the human body.

A typical MR scanner consists of a magnet, gradient coils, shimming coils and radiofrequency (RF) coils together with the control and computer hardware. The magnet produces the main magnetic field $\mathbf{B_0}$ which usually ranges from 0.1 to 3 Tesla for clinical scanners. The main magnet field is produced by a permanent, a resistive or superconductive magnet. This last option is the preferred choice as it achieves higher strength fields. This field is built to be as homogeneous as possible using the shimming coils to correct any inhomogeneity. To achieve spatial localization it is necessary to apply three linear gradient magnetic fields in the x, y and z directions in addition to $\mathbf{B_0}$. These gradient fields, produced by three sets of gradient coils, point in the same direction as $\mathbf{B_0}$ and can be controlled to change in time. When turned on, the resulting magnetic field still points in the direction of $\mathbf{B_0}$ ($\hat{\mathbf{k}}$) but the magnitude depends on the spatial position and is given by

$$\mathbf{B}(x, y, z, t) = \mathbf{B_0} + (G_x(t)x + G_y(t)y + G_z(t)z)\hat{\mathbf{k}} \tag{1.1}$$

The RF coils are used for spin excitation and for the reception of the NMR signals. These coils are usually specific to the part of the human body which will be scanned. This allows to reduce the space between the coil and the anatomy and therefore, to obtain a better image. In some applications, the same coil can be used for both excitation and reception. The control and computer hardware consists of several computers and the electronic equipment necessary to control the scanner. One computer is used to control the scanner, another is used to reconstruct the images and a third computer is the user console which allows the modification of different parameters.

The process to obtain an image can be divided into 4 steps:

- Polarization
- Excitation
- Readout
- Reconstruction

1.1.1. Polarization

The spins within a human body are usually randomly oriented, thus the net macroscopic magnetization ($\mathbf{M}$) is null. If an external magnetic field ($\mathbf{B_0}$) is applied, quantum mechanics states that the spins will take one of two possible orientations, parallel or antiparallel to the external field. The spins are not perfectly aligned with the external field and will experience a torque proportional to it. This torque will produce a precession motion around $\mathbf{B_0}$ at the resonant frequency ω_0 called the Larmor frequency. The Larmor frequency is proportional to the magnetic field and to the gyromagnetic ratio γ as shown in (1.2). The gyromagnetic ratio is constant and unique for each element. For single proton (hydrogen) $\gamma = 42,58$ MHz/T. This means that for a 1.5 Tesla MRI scanner, the Larmor frequency is $63,87$ MHz.

$$\omega_0 = \gamma \cdot B_0 \tag{1.2}$$

After polarization, the spins will have a net macroscopic magnetization greater than zero in the direction of the external field $\mathbf{B_0}$ (Fig. 1.1). This direction is usually called the z-axis and is known as the longitudinal direction. The plane perpendicular to it is known as the transverse plane.

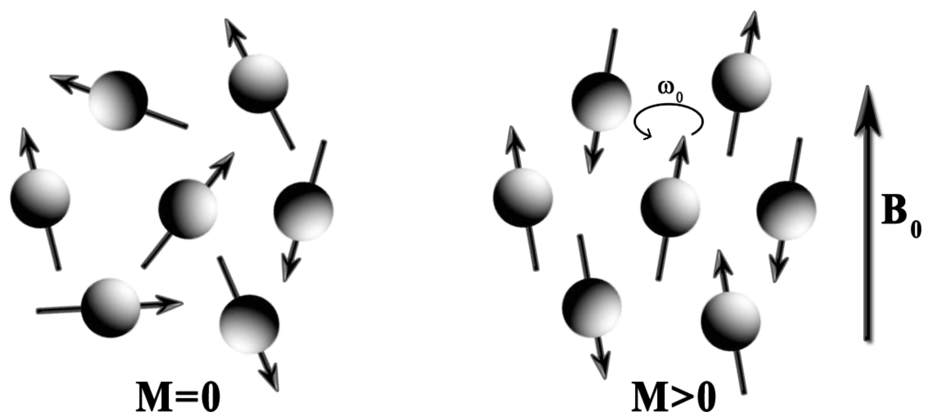

FIGURE 1.1. Polarization of the spins when an external field ($\mathbf{B_0}$) is applied. Left: Spins are randomly oriented in the absence of $\mathbf{B_0}$. Right: Spins are oriented parallel or antiparallel to $\mathbf{B_0}$ and precess at ω_0. A net magnetization $\mathbf{M}$ is produced in the same direction of $\mathbf{B_0}$

1.1.2. Excitation

In this stage, an oscillatory magnetic field B_1 (called RF field) is applied by the RF coil at the Larmor frequency and in the transverse plane. By doing so, the spins absorb energy and get thrown toward the transverse plane while still precessing around the main field $\mathbf{B_0}$. The amount of time the RF field is turned on, and its strength will determine the amount of energy absorbed by the spins. This will finally determine the flip angle in which the spins move toward the transverse plane. If the main field is modified using the gradient fields as in (1.1), spins will have a Larmor frequency that is dependent of their position in space. If the RF pulse B_1 is built to include a particular set of frequencies (by modulating the original signal), it is possible to selectively excite different spins.

1.1.3. Readout

In this stage, the actual data is acquired. After the RF pulse is turned off, the net macroscopic magnetization ($\mathbf{M}$) has been tipped toward the transverse plane. The strength and duration of B_1 determine the flip angle which is optimized to maximize the image contrast. At this point, $\mathbf{M}$ starts to return to its equilibrium position in the longitudinal direction, governed by the Bloch equation (1.3).

$$\frac{d\mathbf{M}(t)}{dt} = \mathbf{M}(t) \times \gamma\mathbf{B}(t) - \frac{M_x\hat{\mathbf{i}} + M_y\hat{\mathbf{j}}}{T_2} - \frac{(M_z - M_0)\hat{\mathbf{k}}}{T_1} \tag{1.3}$$

where M_x, M_y and M_z are the cartesian components of $\mathbf{M}$ and M_0 is the equilibrium magnetization due to $\mathbf{B_0}$; T_1 and T_2 are time constants which define the relaxation rate at which $\mathbf{M}$ recovers its longitudinal magnetization and at which its transverse magnetization decays respectively. Both of these constants are specific to the chemical composition of the acquired substance. During this process, $\mathbf{M}$ still precesses at the Larmor frequency. This precession will induce a voltage in the RF receiver coil due to the Faraday law of electromagnetic induction. Ignoring the T_2 relaxation, the signal equation may be expressed as:

$$s(t) = \int_V m(\mathbf{x})e^{-i\phi(\mathbf{x},t)}d\mathbf{x} \tag{1.4}$$

where $m(\mathbf{x})$ is the density of spins at position $\mathbf{x}$ which have a phase $\phi(\mathbf{x}, t)$. The phase depends on the oscillation frequency (ω) of the spins

$$\phi(\mathbf{x}, t) = \int_0^t \omega(\mathbf{x}, \tau)d\tau = \gamma \int_0^t \mathbf{B}(\mathbf{x}, \tau)d\tau \tag{1.5}$$

which we know is related to the magnetic field through (1.2). Assuming that the field $\mathbf{B_0}$ is homogeneous and that the only other magnetic fields are the linear gradients, using (1.5) and (1.1), (1.4) can be written as:

$$s(t) = e^{-i\gamma B_0 t} \int_V m(\mathbf{x})e^{-i\gamma\mathbf{x}\cdot\int_0^t \mathbf{G}(\tau)d\tau}d\mathbf{x} \tag{1.6}$$

Changing variables and demodulating at $\omega_0 = \gamma B_0$ results in

$$s(t) = \int_V m(\mathbf{x}) e^{-i2\pi \mathbf{k}(t)\cdot\mathbf{x}} d\mathbf{x} \tag{1.7}$$

where

$$\mathbf{k}(t) = \frac{\gamma}{2\pi} \int_0^t \mathbf{G}(\tau) d\tau \tag{1.8}$$

Equation (1.7) states that the signal detected by the receiver coil is the Fourier transform of $m(\mathbf{x})$ which is the density of spins (^1H atoms) at position $\mathbf{x}$. The Fourier domain is presented through $s(t)$ along the trajectory defined by $\mathbf{k}(t)$. This trajectory is called the k-space trajectory as in MRI the frequency domain is called k-space. The k-space trajectory can be changed by modifying the gradient fields $\mathbf{G}(t)$. The strength of $\mathbf{G}(t)$ will determine the speed at which it is possible to move through k-space. Due to hardware cost, security reasons and physical limitations, the maximum gradient strength is limited, thus limiting the speed at which the k-space can be covered.

There are different k-space trajectories such as 2DFT, radial and spiral (Fig. 1.2), being 2DFT the most common. The main reason to choose 2DFT over others is its simplicity for reconstruction as it acquires data on a cartesian grid. Due to the signal decay caused by relaxation, this trajectory reads one line of the k-space at a time. Between each line it is necessary to wait enough time to allow $\mathbf{M}$ to recover its longitudinal magnetization before applying a new excitation. This pause between lines, which can be set by the user through the repetition time (TR), is responsible for significantly increasing the total acquisition time for a whole image whereas the time to cover each line is just a fraction of TR. The direction in which each line is selected is called the *phase encoding direction* whereas the direction in which the line is read is the *readout direction* as it is when the data is actually acquired.

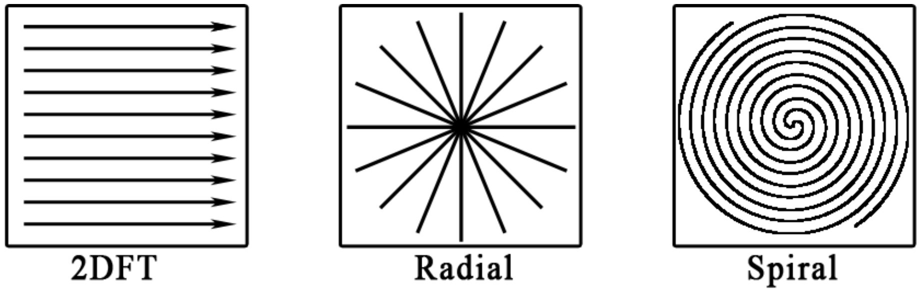

FIGURE 1.2. 2DFT, radial and spiral trajectories used to cover the k-space.

1.1.4. Reconstruction

In this stage, the data acquired is processed to obtain an image of the desired object. If the data was acquired using a cartesian trajectory such as the 2DFT, the reconstruction process is simply applying an inverse discrete Fourier transform to the acquired k-space data. If a noncartesian trajectory is used, it is necessary to remap the acquired data to fit a cartesian grid. In some cases, the data may have been acquired using multiple coils in which the reconstruction will include the use of the coil sensitivities. In order to reduce the acquisition time, the k-space data may have been *undersampled*, thus requiring a more complex reconstruction process.

1.2. Undersampling

A traditional approach to speed up scanning times is to undersample the k-space. This means that instead of sampling the full k-space, only a portion of it is acquired. The amount of data in this portion is quantified through an undersampling factor (The ratio between the number of samples of a fully acquired image over the actual number of acquired samples). A higher undersampling factor means that less data is acquired. In the case of a 2DFT trajectory, the undersampling is done in the phase encoding direction meaning only some lines are acquired. As previously explained, moving from one line to the next is responsible for most of the time spent in acquiring the data. The phase encoding direction can be chosen, so lines may be rows or columns. To understand undersampling and its effects, it is necessary to understand what the meaning of *full k-space* is. In standard MRI

$$\Delta k = \frac{1}{FOV} \tag{1.9}$$

where FOV stands for Field of view.

The Nyquist sampling theorem states that the uniform spacing between samples Δk in k-space must be smaller or equal to the inverse of the field of view which will be reconstructed. If this criteria is not met, the image will not reconstruct properly and will be subject to blurring, ringing or aliasing artifacts. Using the same principle, it is possible to calculate the resolution of an image (Δx) as:

$$\Delta x = \frac{1}{2k_{max}} \tag{1.10}$$

By undersampling, the Nyquist theorem is not met so it is not possible to apply the inverse Fourier transform directly without producing artifacts that depend on the used undersampling pattern (Fig. 1.3). Some sort of prior information must be used to reconstruct the missing data. One example is the use of the partial matrix technique, which reconstructs the image based on the assumption that it is real (not complex) and therefore its Fourier transform would be hermitian. This would allow to acquire only half of the k-space and the other half can be easily reconstructed by symmetry. However, there is always some degree of field inhomogeneities and other factors so that the final reconstruction will always show some artifacts.

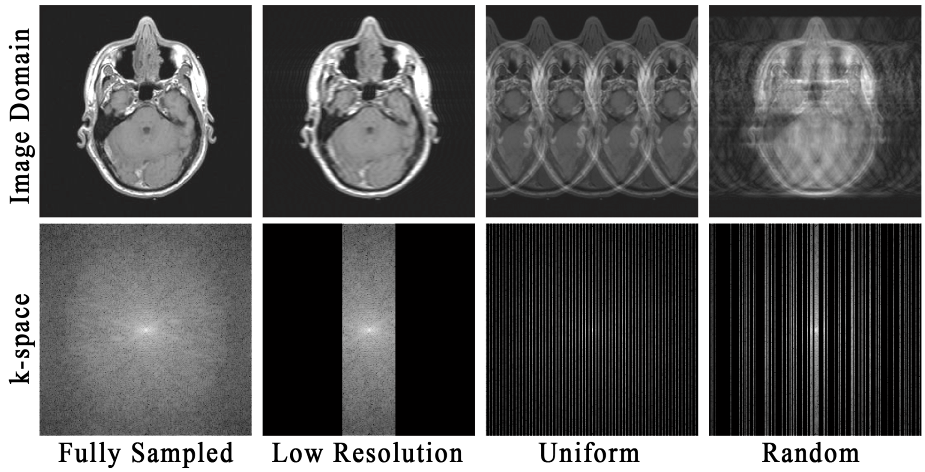

FIGURE 1.3. Artifacts produced by undersampling the k-space with an undersampling factor of 4 in the phase encoding direction of a 2DFT. The fully sampled image is presented with its corresponding k-space. A low resolution image is obtained when the center of the k-space is acquired. The image is replicated and overlapped if a uniform undersampling pattern is used. The image presents less coherent artifacts for a random undersampling pattern.

2. INTRODUCTION

Currently, MRI is the chosen medical imaging technique for many clinical studies. However, the application of MRI to three-dimensional (3D) and dynamic data is still a challenge due to the long acquisition times involved. Over the last years, several strategies have been proposed to speed up the scanning time in MRI, without sacrificing spatial or temporal resolution. This has been achieved by designing more efficient sequences and trajectories which provide faster coverage of the k-space (Carr, 1958; Stehling et al., 1991; Irarrazabal & Nishimura, 1995; Thedens et al., 1999); by using parallel imaging methods which employ the spatial sensitivity of multiple coils as a complementary encoding information (Sodickson & Manning, 1997; Pruessmann et al., 1999; Griswold et al., 2002); and by developing methods for reconstructing images from undersampled data. The idea of such reconstruction algorithms is to reduce the number of acquired samples and estimate the non-acquired ones by using some prior information or extra assumptions.

Most of the undersampled reconstruction techniques exploit some kind of redundancy (i.e. k-space redundancy, temporal redundancy or both) or take advantage of prior information. Those methods include keyhole (Jones et al., 1993; Vaals et al., 1993), reduced Field of View (rFOV) (Hu & Parrish, 1994), UNaliasing by Fourier-encoding the Overlaps using the temporaL dimension (UNFOLD) (Madore et al., 1999), vastly undersampled isotropic voxel radial projection imaging (VIPR) (Barger et al., 2002), k-t Broad-use Linear Acquisition Speed-up Technique (k-t BLAST)(Tsao et al., 2003), reconstruction employing temporal registration (Irarrazaval et al., 2005), HighlY constrained backPRojection (HYPR)(Mistretta et al., 2006), reconstruction of undersampled dynamic images by modeling the motion of objects elements (Prieto et al., 2007); and combinations of parallel imaging with other techniques, such as k-t SENSE (Tsao et al., 2003), adaptive sensitivity encoding incorporating temporal filtering (TSENSE) (Kellman et al., 2001), UNFOLD-SENSE (Madore, 2004), TGRAPPA (Breuer et al., 2005) and k-t GRAPPA (Huang et al., 2005). Other recent approach to reconstruct undersampled images is based in the compressed sensing theory (Candes et al., 2006; Donoho, 2006). Those techniques exploit the sparsity and compressibility of the MRI images. Some of the methods based on this approach are found in (Lustig et al., 2007; Jung et al., 2007; Ye et al., 2007; Block et al., 2007).

The main problem with most of the known reconstruction algorithms is that they are prone to introduce spatial or temporal blurring due to the use of low resolution images or temporal averages in the reconstruction. For example, keyhole initially acquires a full k-space but then only updates the central region of the k-space. By doing so, small image regions which change their intensity and fall outside of the updated k-space region will not be reconstructed, thus introducing spatial blurring. Another example is sliding window (d'Arcy et al., 2002) in which different portions of k-space are acquired in different time frames. The reconstruction is based on the fact that the temporal variations of k-space are smooth and therefore missing data can be reconstructed by interpolation. By doing so, sliding window is prone to introduce temporal blurring.

The main objective in this thesis is to present a new reconstruction method for undersampled data that is able to reduce both the spatial and temporal blurring. The new Technique for Reconstruction based on the Intensity Order (TRIO) is presented, which uses an estimation of the image intensity order as prior information. We define the *intensity order* as the information which allows sorting the pixels of an image from brightest to darkest. Importantly, this prior information does not relate directly with the signal intensities of the object, but only with the order relation of those intensities. With such information it is possible to transform an image domain into a sorted domain. This information is strong enough to allow the reconstruction of undersampled data. If the estimated image, with its intensity values, which are obviously not the correct ones, are used as prior information, one risks the possibility of propagating those error into the final reconstruction. That is the motivation for discarding the actual intensity values and using only the intensity order. Relaxation of the intensity order can be done to further improve the quality of the prior information.

3. METHODS

3.1. Intensity Order

The main hypothesis of our method is that the intensity order information is powerful enough to allow the reconstruction of undersampled images. Let us define the intensity order information as a series of relations between pixels in which each relation states which pixel is brighter and which is darker. These relations are defined through inequalities such as

$$x_a \geq x_b \quad \text{states that the pixel at position } a \text{ is } \textit{at least as bright} \text{ as pixel at position } b. \tag{3.1}$$

and will be called intensity order information.

Let Ω be the whole set of relations for an entire image which defines the intensity order information. Importantly, Ω never includes the actual intensity values, but only such relations. To sort an image correctly from brightest to darkest (Fig. 3.1), Ω must be *complete* and *accurate*. The relation between all combinations of pairs of pixels must be defined in order to consider Ω to be *complete*. This demands $\binom{N}{2}$ inequalities for an image with N pixels, although only $N-1$ inequalities are required because the remaining relations are automatically defined by transitivity. For Ω to be considered *accurate*, every relation must show no conflict with the actual intensity values of the fully sampled image. For example, a complete and accurate definition of Ω for the sorting process shown in Fig. 3.1 is given in (3.2), in which the complete set of $\binom{8}{2}$ inequalities are defined with their corresponding reduced set of $(8-1)$ inequalities obtained by transitivity.

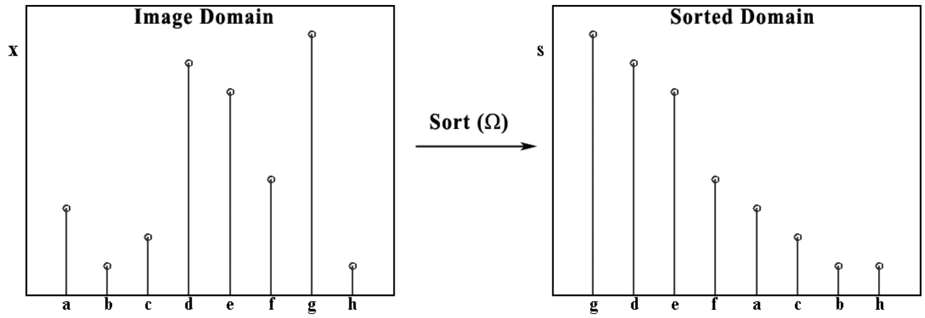

FIGURE 3.1. Example of the sorting process for an 8-point signal. Left: Original (unsorted) signal. Right: Sorted signal using information provided in Ω.

$$\Omega = \begin{cases} x_g \geq x_a \;\; x_g \geq x_b \;\; x_g \geq x_c \;\; x_g \geq x_d \;\; x_g \geq x_e \;\; x_g \geq x_f \;\; x_g \geq x_h \\ x_d \geq x_a \;\; x_d \geq x_b \;\; x_d \geq x_c \;\; x_d \geq x_e \;\; x_d \geq x_f \;\; x_d \geq x_h \\ x_e \geq x_a \;\; x_e \geq x_b \;\; x_e \geq x_c \;\; x_e \geq x_f \;\; x_e \geq x_h \\ x_f \geq x_a \;\; x_f \geq x_b \;\; x_f \geq x_c \;\; x_f \geq x_h \\ x_a \geq x_b \;\; x_a \geq x_c \;\; x_a \geq x_h \\ x_c \geq x_b \;\; x_c \geq x_h \\ x_b \geq x_h \end{cases} = \begin{cases} x_g \geq x_d \\ x_d \geq x_e \\ x_e \geq x_f \\ x_f \geq x_a \\ x_a \geq x_c \\ x_c \geq x_b \\ x_b \geq x_h \end{cases} \tag{3.2}$$

When the true intensity order information is not available and needs to be estimated, there is in general a trade-off between completeness and accuracy. If Ω is complete but not accurate, it is possible to remove relations between pixels to make it more accurate but loosing completeness in the process. On the other hand, if the information is incomplete, it is possible to arbitrarily define the missing relations to complete Ω but sacrificing accuracy. We shall call Ω_c to any complete set of relations built from an originally incomplete set Ω.

3.2. Minimization

The proposed method uses the intensity order information to compensate for the loss of image information due to undersampling. The reconstruction is done through an ℓ_2-norm minimization to reduce the data consistency error between the reconstructed image and the acquired data, but bound by the constraints given by the intensity order information supplied by Ω. The general reconstruction algorithm is therefore defined as

$$\begin{aligned} &\mathbf{Min} \left\| \mathbf{W}^H \cdot \mathbf{U} \cdot \mathbf{W}\mathbf{x} - \mathbf{y} \right\|^2 \\ &s.t.\ \Omega \end{aligned} \tag{3.3}$$

where $\mathbf{x}$ is the unknown variable that represents the intensity values of the image, $\mathbf{W}$ is the Fourier transform operator, $\mathbf{U}$ is the under-sampling pattern and $\mathbf{y}$ is the aliased acquired image.

For a complete and accurate set Ω, let $\mathbf{P}$ be the permutation operator constructed from such information allowing to sort the pixels of image $\mathbf{x}$ in intensity descending order. Knowing $\mathbf{P}$, the sorted domain $\mathbf{s}$ is given by

$$\mathbf{s} = \mathbf{P} \cdot \mathbf{x} \tag{3.4}$$

Writing (3.3) in terms of $\mathbf{s}$ lead us to

$$\begin{aligned} &\mathbf{Min} \left\| \mathbf{W}^H \cdot \mathbf{U} \cdot \mathbf{W} \cdot \mathbf{P}^T \mathbf{s} - \mathbf{y} \right\|^2 \\ &s.t.\ \forall i > j :\ s_i \geq s_j \end{aligned} \tag{3.5}$$

where $\mathbf{s}$ becomes the new unknown variable that replaces $\mathbf{x}$ through (3.4), defining the sorted image domain. This change is done to simplify the formulation of the constraints for the minimization problem (now the constraints can easily be written as inequalities).

The true order information is in general not available, and therefore it needs to be estimated. An approximation of a complete Ω can be easily estimated but it would probably be inaccurate. A complete but inaccurate order information applied to the constraints of the minimization problem would cause the reconstruction to fail. To avoid this, it is necessary to relax the constraints by building an incomplete but more accurate version of Ω, giving some freedom to the optimization variables. This freedom allows the pixels to take an intensity value which would change their original positions in the sorted domain.

This is done by creating disjoint groups (named α_k) of n pixels each and defining the relations between every two groups. The relations between pixels within each group is left undefined so that every pixel has a limited scope where it can move without constraints (Fig. 3.2). In the modified minimization problem defined as

$$\begin{aligned} &\mathbf{Min} \left\| \mathbf{W}^H \cdot \mathbf{U} \cdot \mathbf{W} \cdot \mathbf{P}^T \mathbf{s} - \mathbf{y} \right\|^2 \\ &s.t.\ min\left\{s \in \alpha_k\right\} \geq max\left\{s \in \alpha_{k+1}\right\} \text{ for } 1 \leq k \ \leq \frac{N}{n} - 1 \end{aligned} \tag{3.6}$$

Ω is incomplete so $\mathbf{P}$ has to be built from a complete (but inaccurate) version Ω_c. If the group size n is set to one, then the problem is reduced to the perfectly known order information case, where (3.5) applies.

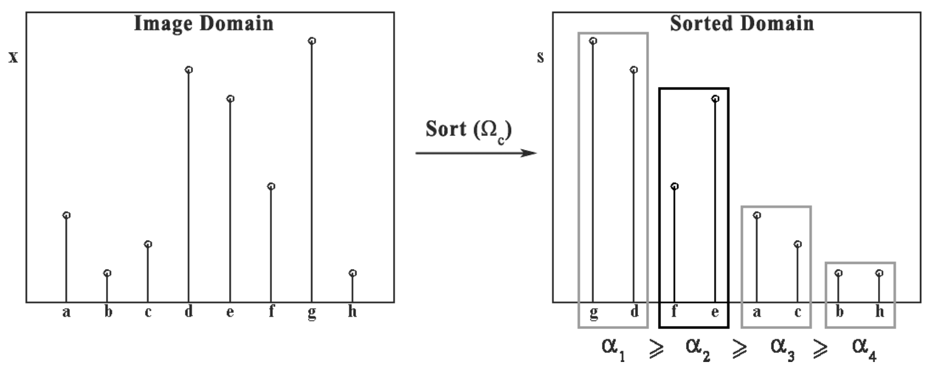

FIGURE 3.2. Example of the relaxed sorting process for an 8-point signal. The original signal is sorted using a complete but innacurate Ω_c to construct P, which produces a mistake in the signal in the sorted domain at the right. Four groups are created for every n=2 pixels. Pixels in $\alpha_1 \geq \alpha_2 \geq \alpha_3 \geq \alpha_4$. These last relations are incomplete as they do not define the relations between all pixels, but they are accurate.

The fact that an inaccurate Ω_c was used to construct P means that the sorting process is in general wrong. It is possible however to correct such mistakes defining the constraints of the minimization problem with disjoint groups α_k.

The minimization of the data consistency error (3.6) is done in the image domain rather than in Fourier space to improve convergence. The optimum is the best estimation of the actual intensity value for each pixel, bound by the order information constraints. The initial intensity values for the minimization must be different from those used to obtain the order information. A natural way to do so is to set the initial values to zero. Obviously, if the order information is complete and accurate the undersampling factor can be increased.

3.3. Estimation of the sorted domain

Reasonable estimations of the sorted domain can be obtained from low resolution images, statistics learned from training data, adjacent slices in volumetric images, temporal correlation in dynamic sequences, and images reconstructed with other conventional algorithms for undersampled data. In this last case, TRIO can be applied as a second stage to overcome the problems of the previous reconstructions (spatial or temporal blurring) improving the overall quality of the image.

As previously stated, any mistake in the estimation of the sorted domain will produce errors in the reconstruction, which can be solved by increasing the size n for each disjoint group α_k. For example, when taking a low resolution (60% of k-space) version of a particular image it generates an Ω with a 16.8% of wrong relations when checked with the fully sampled image. If n is increased to 4 and 8, this value decreases to 7.7% and 4.5% respectively. When using the adjacent slice of such image to contruct Ω, errors of 22.2%, 19.3% and 16.0% are obtained for group sizes of 1, 4 and 8 respectively. If the slice thickness of the acquired image is reduced, adjacent slices would be more similar and would reduce the errors of Ω. If TRIO is used as a second stage reconstruction, then the quality of the estimated sorted domain will depend on the quality of the reconstruction achieved by the previous algorithm. By increasing the group size in this case, some of the errors produced by the first method will be avoided, thus allowing TRIO to improve the first stage reconstruction.

3.4. Experiments

The proposed reconstruction algorithm was tested in 2D static and dynamic images. Fully sampled images were acquired and subsequently undersampled retrospectively using uniform, cartesian random and pseudo random undersampling patterns. Three experiments were performed differing mainly on the source of the order information.

3.4.1. Experiment I

To prove the feasibility of using order information, 2D static images were first reconstructed using the order information from the fully sampled image which means that a complete and accurate Ω was supplied. This test was repeated for undersampling factors of 4, 8, 16 and 32 and for group sizes (n) of 4, 8 and 16 pixels. In this case a random undersampling pattern in the phase-encoding direction was used, but always ensuring that the center of the k-space was acquired. The two fully sampled images used for this experiments are shown in Fig. 3.3. The second image was used to show that TRIO is independent of the sparsity of the image domain.

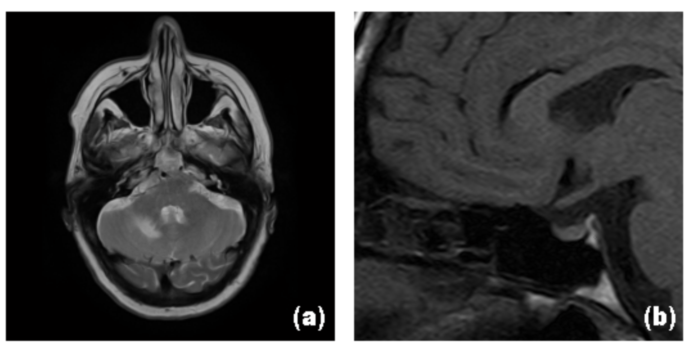

FIGURE 3.3. The two fully sampled images that were used to test the feasibility of using the order information to reconstruct undersampled data. **(a)** T2W-TSE Axial Brain image. **(b)** Portion of a T1W-SE sagittal brain image

The first image is a T2 weighted turbo spin echo (T2W-TSE) axial brain image acquired with a Philips Achieva 1.5T, TR/TE $=$ 4438 ms/100 ms, FOV $= 230 \times 230$ mm^2, flip angle = 90°, resolution = 0.9×0.9 mm^2, slice thickness = 5 mm, acquisition matrix = 256×256, TSE factor = 15.

The second image is a 256×256 portion of an originally larger image. The original image is a T1 weighted spin echo (T1W-SE) sagittal brain image acquired with a Philips Intera 1.5T, TR/TE = 400 ms/15 ms, FOV = 180×180 mm^2, flip angle = 90°, resolution = 0.35×0.35 mm^2, slice thickness = 3 mm, acquisition matrix = 512×512.

3.4.2. Experiment II

In this experiment a set of 2D dynamic cardiac images were used. The raw data was undersampled retrospectively by employing a pseudo-random pattern with a factor (Q) of 4. This pattern is random in k-space and uniform in time, i.e. all lines in k-space are acquired once every Q frames. The order information from the temporal average of the undersampled dynamic sequence was used to estimate Ω for the first frame. For the remaining frames, Ω was built using the order information of the pixels from the reconstructed previous frame as shown in Fig. 3.4. Images were reconstructed with TRIO using a group size of 4 pixels.

The images were acquired in a Philips Intera 1.5T using a 2D balanced fast field echo (B-FFE) cardiac-gated sequence, TR/TE = 3 ms/1.46 ms, FOV = 400×320 mm^2, flip angle = 50°, resolution = 1.56×2.08 mm^2, slice thickness = 8 mm, acquisition matrix = 256×154, 50 frames, five channel cardiac coil, and breath-hold duration close to 25s. The parallel acquisition from the five coils was first reconstructed using SENSE (Pruessmann et al., 1999) to obtain the set of images that were used in this experiment.

3.4.3. Experiment III

TRIO was also tested as a second stage reconstruction to improve the performance of keyhole, k-t BLAST and sliding window. In every case, Ω was constructed from the intensity values obtained from the first stage reconstruction as shown in Fig. 3.5. The images were compared before and after applying TRIO as a second stage. For this experiment we

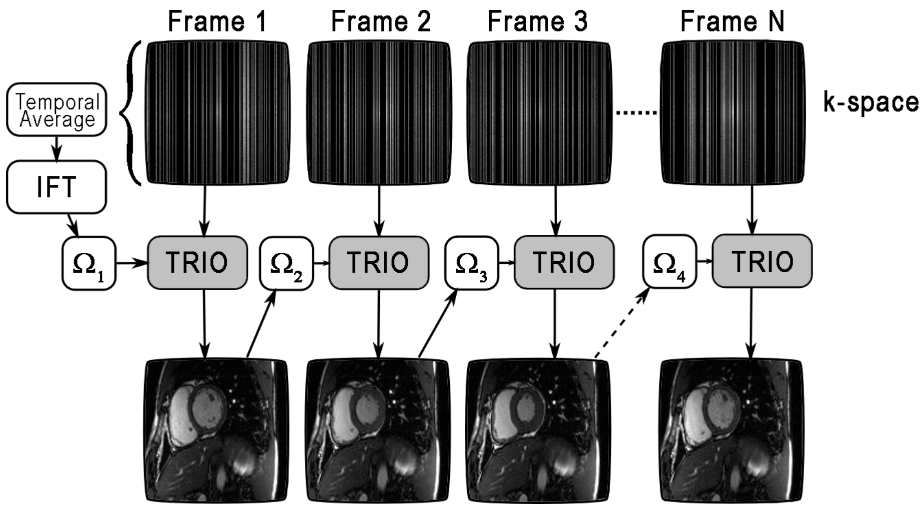

FIGURE 3.4. Dynamic sequence reconstruction using TRIO. The temporal average image computed in the Fourier domain is used to estimate the order information (Ω_1) for the first frame. Using Ω_1 and the corresponding undersampled data allows TRIO to reconstruct the first frame. The second frame is reconstructed using Ω_2 which is obtained from the first frame and its k-space data. Every following frame is reconstructed using the estimated order information from the previous frame combined with its own undersampled k-space data.

used the same set of 2D dynamic cardiac images as in experiment II and the same pseudo-random undersampling pattern. The uniformity in time of the undersampling pattern is required to allow good reconstructions when using k-t BLAST and sliding window.

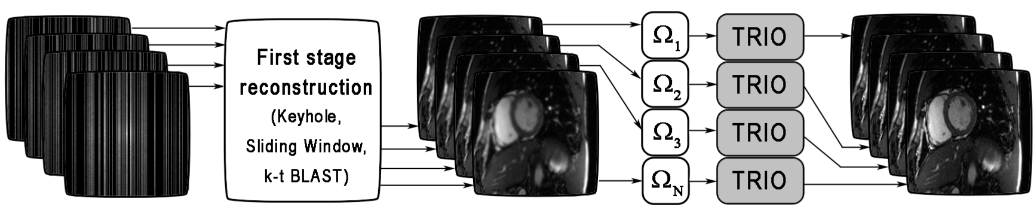

FIGURE 3.5. TRIO used as a second stage reconstruction to keyhole, k-t BLAST or sliding window. The actual intensity values obtained from the first stage reconstructions are discarded while keeping the order information necessary to construct Ω.

For a fair comparison, the data was also reconstructed using k-t BLAST with a uniform under-sampling pattern. For keyhole and k-t BLAST, 18 extra central phase-encoding lines were collected for each time frame with which a net undersampling factor of 3.7 was achieved. The k-t BLAST algorithm was implemented using a conjugate gradient method (Hansen et al., 2006).

4. RESULTS

4.1. Experiment I

As Figs. 4.1 and 4.2 show, TRIO can reconstruct without a noticeable loss in image quality with an undersampling factor of 4x and group sizes (n) of 1, 4 and 8 pixels. When using an undersampling factor of 8 it is possible to achieve a good reconstruction when the group size is set to 1 pixel for the axial brain dataset (Fig. 4.1) and up to n=8 for the sagittal brain dataset (Fig. 4.2). Increasing the undersampling factor or n results in artifacts in the phase encoding direction. A closer look to one line of the axial brain image reconstructed with 8x and n=1 is presented in Fig. 4.3.

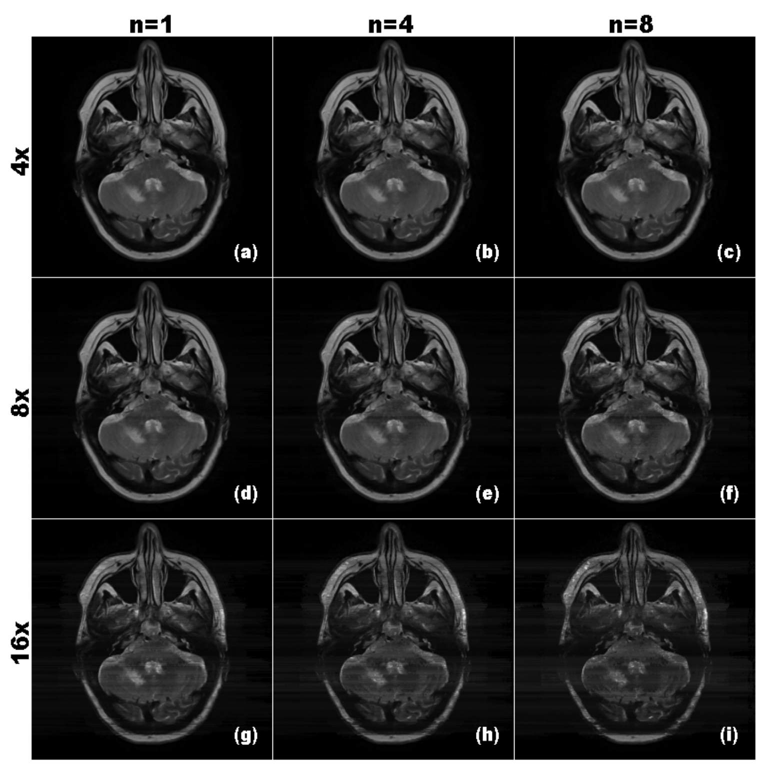

FIGURE 4.1. Reconstruction of the axial brain image (Fig. 3.3a) using TRIO with a complete and accurate Ω. Results for undersampling factors of 4x, 8x and 16x combined with group sizes (n) of 1, 4 and 8 pixels.

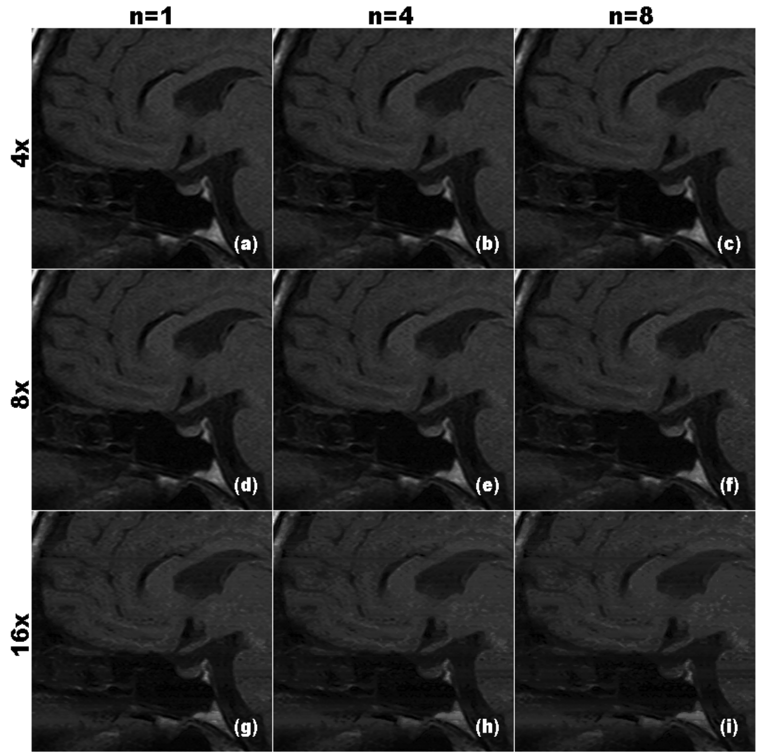

FIGURE 4.2. Reconstruction of the sagittal brain image (Fig. 3.3b) using TRIO with a complete and accurate Ω. Results for undersampling factors of 4x, 8x and 16x combined with group sizes (n) of 1, 4 and 8 pixels.

From tables 4.1 and 4.2 it is possible to verify quantitatively that TRIO produces good results for 4x even with a group size of 16. The results show a better reconstruction for the sagittal brain data set (Fig. 3.3b) than for the axial brain data set (Fig. 3.3a) which suggests that the image does not need to be sparse in the image domain for the algorithm to work properly.

4.2. Experiment II

As can be seen in Fig. 4.4 (only two representative frames are included) the difference between the fully sampled data and the TRIO reconstruction shows that the main errors are produced on the edges of the left ventricle, although these are very low, specially for

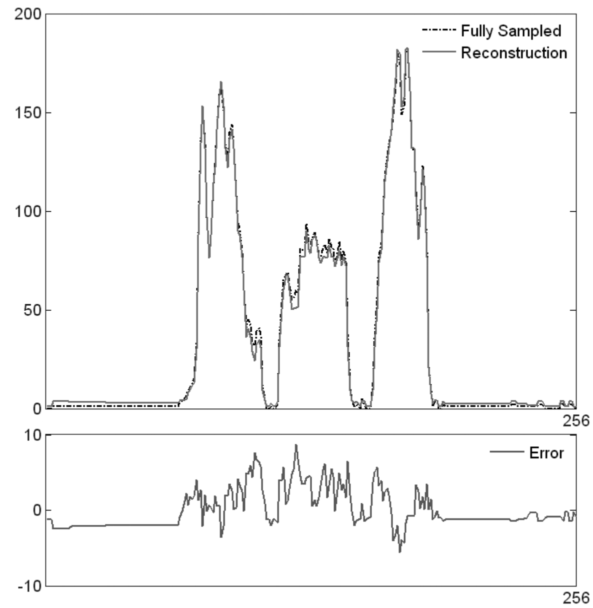

FIGURE 4.3. One line of the reconstruction of the axial brain image (Fig. 3.3a) using 8x and n=1. The error between the reconstructed and fully sampled image is also shown.

RMS error[%]

	$n = 1$	$n = 4$	$n = 8$	$n = 16$
$4x$	0.1	0.3	0.5	0.9
$8x$	1.2	1.9	2.9	4.6
$16x$	4.3	5.9	7.6	9.5
$32x$	8.9	10.8	12.6	14.4

TABLE 4.1. Root mean square (RMS) errors in percentage for reconstructions shown in Fig. 4.1 compared to the fully sampled image. The values for a group size of $n = 16$ and for an undersampling factor of 32x are also included.

RMS error[%]

	$n = 1$	$n = 4$	$n = 8$	$n = 16$
$4x$	0.1	0.3	0.5	0.8
$8x$	0.7	1.0	1.4	2.1
$16x$	2.3	2.8	3.3	4.0
$32x$	6.1	6.7	7.2	7.6

TABLE 4.2. Root mean square (RMS) errors in percentage for reconstructions shown in Fig. 4.2 compared to the fully sampled image. The values for a group size of $n = 16$ and for an undersampling factor of 32x are also included.

frame 2. Quantitatively, we found that the root mean square (RMS) error for the whole sequence when compared to the fully sampled data was 0.74%.

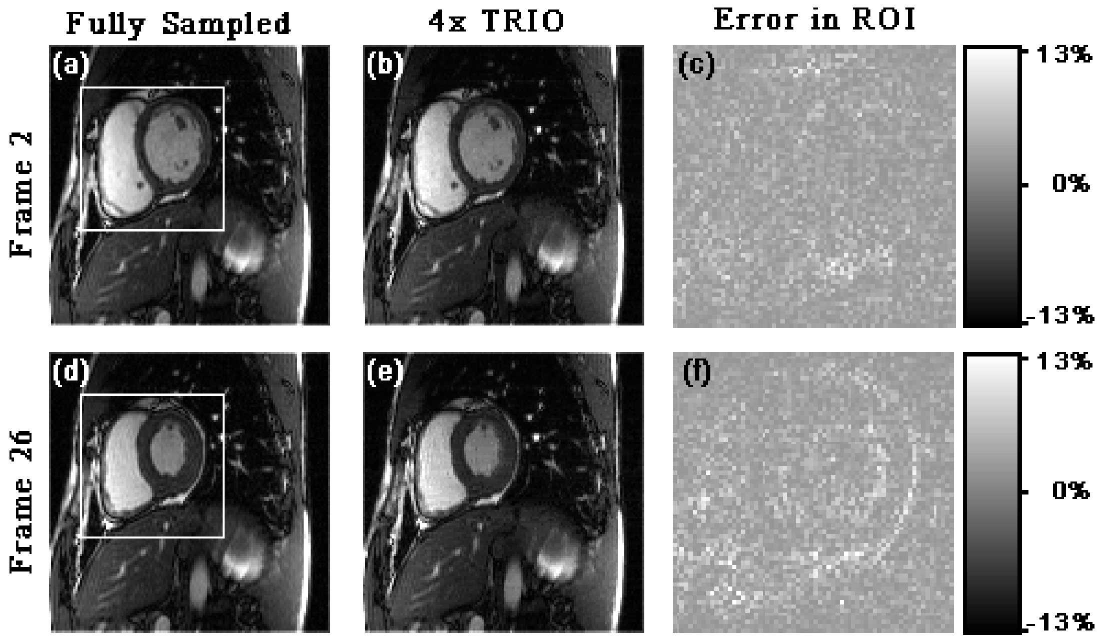

FIGURE 4.4. 4x TRIO reconstruction for 2 representative frames of the cardiac sequence with their respective difference image for a region of interest (ROI). The order information for the first frame is obtained from the temporal average while every frame provides the order information for the next frame. **(a)** Fully sampled image for frame 2. The white rectangle marks the ROI. **(b)** Reconstructed image using TRIO for frame 2. The order information is obtained from frame 1. **(c)** Difference image between the ROI in (a) and (b) windowed to reveal the details. **(d)** Fully sampled image for frame 26. The white rectangle marks the ROI. **(e)** Reconstructed image using TRIO for frame 26. The order information is obtained from frame 25. **(f)** Difference image between the ROI in (d) and (e) windowed to reveal the details.

By plotting the temporal evolution of a particular line across the left ventricle (Fig. 4.5), it is possible to note that TRIO introduces negligible temporal blurring.

4.3. Experiment III

As can be seen from Fig. 4.6, TRIO improves the reconstruction achieved by keyhole, sliding window and k-t BLAST (Figs. 4.6b, 4.6c and 4.6d respectively) when it is applied

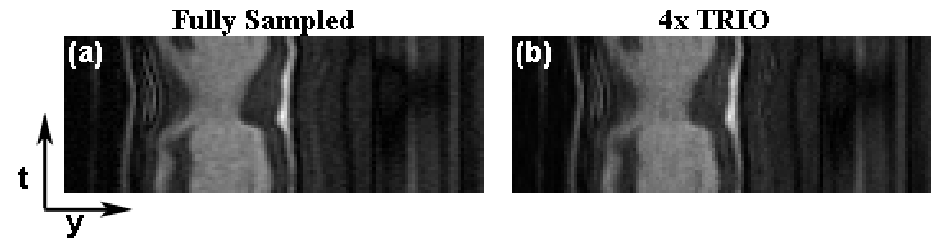

FIGURE 4.5. Temporal evolution along the y-axis across the left ventricle for (a) the fully sampled sequence and (b) 4x TRIO reconstruction.

as a second stage reconstruction (Figs. 4.6f, 4.6g and 4.6h). Remarkably, TRIO allows to reduce the errors on edges and spatial blurring produced by the alternative methods.

As can be seen from Fig. 4.7, after TRIO is applied, it reduces the RMS errors for all frames when compared to keyhole, sliding window and k-t BLAST (with uniform and random undersampling).

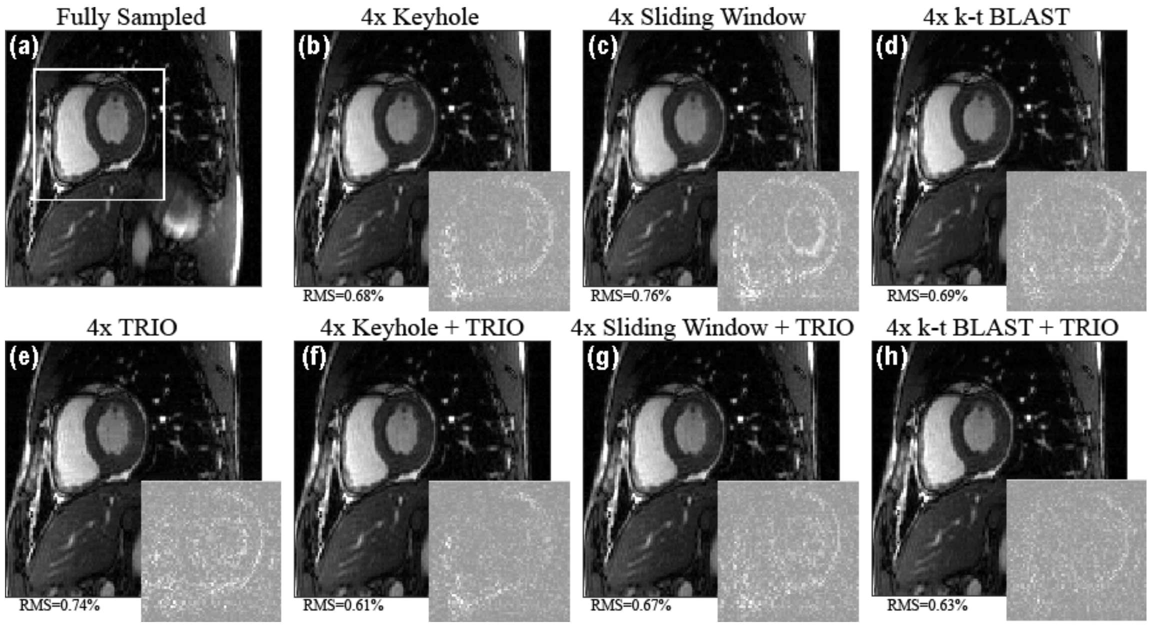

FIGURE 4.6. TRIO reconstruction for frame 26 of the 2D cardiac sequence compared to keyhole, k-t BLAST and sliding window with their respective RMS errors and difference image of a ROI. The RMS error presented corresponds to the complete sequence. **(a)** Fully sampled image. The white rectangle marks the ROI. **(b)** 4x reconstruction using keyhole. **(c)** 4x reconstruction using sliding Window. **(d)** 4x reconstruction using k-t BLAST. **(e)** 4x reconstruction using TRIO as in experiment II. The order information for the first frame was obtained from the temporal average. Each frame provides the order information for the next frame. **(f)** TRIO reconstruction using (b) as the order information. **(g)** TRIO reconstruction using (c) as the order information. **(h)** TRIO reconstruction using (d) as the order information.

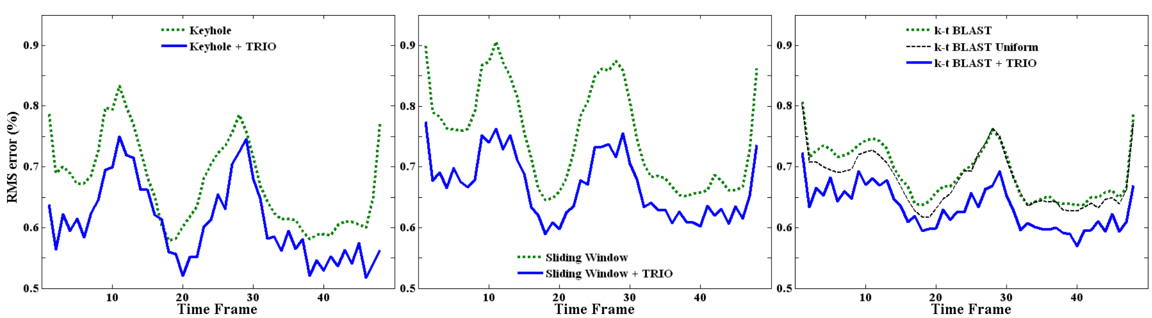

FIGURE 4.7. Temporal evolution of the RMS error for TRIO when used as a second stage reconstruction compared to the first stage methods.

5. DISCUSSION

The results show that the proposed method is able to reconstruct the images from undersampled static and dynamic sequences with an RMS error no greater than 0.74% when using an undersampling factor of 4. Furthermore, the error produced by the reconstruction using TRIO is less structured, achieving less spatial and temporal blurring than traditional undersampled reconstruction techniques.

The fact that the prior information used for the reconstruction is obtained from the image domain and that it is as simple as the relations between the intensity of every pixel makes it possible to easily obtain such information. The use of order information differs from the traditional use of prior information because it discards the actual intensity value. This would be similar to having a perfectly intensity equalized version of the image. The use of the ℓ_2-norm favors the error to be scattered across all pixels rather than having big errors in a specific pixel or set of pixels. By combining this with the transformation between the sorted and the image domains it is possible to reduce the structure in the errors. The result is a noise-like error spread over the whole image.

The results showing a low spatial and temporal blurring prove that even by using the temporal average as a starting point, TRIO is able to avoid the introduction of significant temporal blurring. This also validates the use of prior frames as a valid source for the estimation of the order information.

The results also show that TRIO can be used as a second stage reconstruction to keyhole, k-t BLAST and sliding window. With TRIO, it is also possible to observe less structured errors in the reconstructed image, particularly in edges which were blurred by the alternatives or previous reconstruction methods. This was true for random or pseudo random undersampling pattern and also for a uniformly spaced undersampling pattern considered for k-t BLAST.

The results of applying TRIO as a second stage reconstruction show that the quality of the reconstruction is dependent on the accuracy of the estimated order information used to construct Ω. The errors incorporated during the estimation of such information in the first stage reconstruction are inherited by TRIO, but the errors are subsequently reduced by creating a group size greater than 1, allowing to improve the reconstruction. However, increasing the group size much further would result in poor reconstruction as shown in Figs. 4.1 and 4.2.

The high computational load of this technique is a problem, and has limited its use to undersampling in the phase encoding direction but with full readouts. This allows the reconstruction to be done one line at a time, greatly reducing the number of simultaneous variables. For a 256×256 image this reduces the amount of variables (pixels) calculated at any given time from 65536 to 256 thus allowing the problem to become manageable. The problem with this approach is that it does not allow full 2D undersampling patterns which greatly reduce the coherence in the aliased image and would allow the reconstruction of 3D images. To reduce the computational load it is necessary to reduce the amount of constraints which are the same as the number of pixels in the image for the best case scenario (when the group size $n = 1$). To achieve this, some work has been done to parameterize the smooth curve obtained by sorting the image as in the example shown in Fig. 3.1. For an image of 65536 pixels (256×256) it is possible to describe accurately such curve with a parametric curve (e.g. B-splines) with nearly 30 parameters. Using this approach, TRIO is able to reconstruct with a negligible error an image with a 16x 2D undersampling pattern. Furthermore, the reconstruction is done in just a few seconds instead of 3 to 7 hours as the original method. However, this last approach carries the problem that it has not yet been possible to include an equivalent to the group size to allow freedom to the pixels. This is necessary if an inaccurate order information is supplied. Further work is being done to overcome this problem in order to be able to apply this promising results to real cases.

While writing this thesis, we noticed that another research team has also used similar concepts relating to intensity order in under-sampled image reconstruction (Adluru &

DiBella, 2008). They use an approach in which the intensity order helps to improve the convergence of the minimization problem in a Compressed Sensing framework.

6. CONCLUSIONS

A Technique for Reconstruction using Intensity Order (TRIO) has been proposed. The method allows to reconstruct undersampled images using an estimation of the intensity order information. This information is used to construct the constraints to a minimization problem that provides the consistency to the acquired data. Such constraints are relaxed to allow some movement between the pixels within a group to correct errors in the estimation of the order information. The estimation is easily obtained from low resolution images, adjacent slices, prior reconstructions, temporal average or prior frames. The feasibility of using order information to reconstruct was proved by reconstructing 2D static images with different undersampling factors and group sizes to relax the constraints. These reconstruction were done providing TRIO with the correct order information. The method was then tested using a 2D cardiac sequence with an undersampling factor of 4. Such reconstruction was compared to keyhole, sliding window and k-t BLAST. The source for the prior information was obtained from temporal averaging and prior frames for one experiment. Other experiments were done where TRIO was applied using the order information estimated by the reconstruction achieved by the other techniques. In every case TRIO shows an improvement in the reconstruction by reducing both spatial and temporal blurring. This improvement is shown by a reduced root mean square error and a less structured error. The high computational load is a problem that limits the use of this algorithm, but ongoing work has proved that higher undersampling factors can be achieved using the same order information if this problem is solved. This would allow the use of this method in 3D imaging with 16 or greater undersampling factors.

7. FUTURE WORK

The high computational load of the proposed method is the main obstacle to be solved. Once this problem is solved, the method can be easily applied to 3D imaging and higher undersampling factors can be achieved. Different strategies are proposed to reduce the computational burden.

- Improve the efficiency of the optimization code to reduce the high memory consumption of the current code without overloading the CPU.
- Continue the work with the use of B-splines to describe the image in the sorted domain to reduce the amount of variables in the minimization problem. The main problem with this approach, that has not yet been solved, is to include the ability to introduce some flexibility to the constraints, allowing the algorithm to correct the errors inherited by the use of incorrect order information.
- A similar approach as that using B-splines, is to describe the smooth curve produced in the image domain using only the central Fourier coefficients of such curve. The missing flexibility is still the main problem with this approach.
- Include the use of equalities in the constraints besides the exclusive use of inequalities. The idea is to group all pixels which should be similar in intensity (such as a black background) in only one variable.
- Look for new ways of reducing the total amount of variables without sacrificing the required flexibility in the constraints.

In addition to reducing the computational load, two new approaches which involve variations in the use of the order information are proposed.

- The use of order information as prior information is very similar as using an intensity equalized version of the image. In fact, using the order information and assigning a linearly decreasing value from the brightest pixel to the darkest constructs an equalized version of the image. The use of the equalized image as prior information should be further investigated.

- In the same line of investigation, the maximization of the mutual information between the equalized image (constructed from the intensity order information) and the reconstructed image could also be used, instead of explicitly defining the order constraints.

REFERENCES

Adluru, G., & DiBella, E. (2008). Data reordering for improved constrained reconstruction from undersampled k-space data. In *Proceedings* 16^{th} *ismrm scientific meeting* (p. 3153). Toronto, Canada.

Barger, A. V., Block, W. F., Toropov, Y., Grist, T. M., & Mistretta, C. A. (2002). Time-resolved contrast-enhanced imaging with isotropic resolution and broad coverage using an undersampled 3D projection trajectory. *Magnetic Resonance in Medicine*, *48*(2), 297-305.

Bloch, F. (1946, Oct). Nuclear induction. *Phys.Rev.*, *70*(7-8), 460-474.

Block, K. T., Uecker, M., & Frahm, J. (2007). Undersampled radial MRI with multiple coils. iterative image reconstruction using a total variation constraint. *Magnetic Resonance in Medicine*, *57*(6), 1086-1098.

Breuer, F. A., Kellman, P., Griswold, M. A., & Jakob, P. M. (2005). Dynamic autocalibrated parallel imaging using temporal GRAPPA (TGRAPPA). *Magnetic Resonance in Medicine*, *53*(4), 981-985.

Candes, E. J., Romberg, J., & Tao, T. (2006). Robust uncertainty principles: exact signal reconstruction from highly incomplete frequency information. *Information Theory, IEEE Transactions on*, *52*(2), 489-509.

Carr, H. Y. (1958, Dec). Steady-state free precession in nuclear magnetic resonance. *Phys.Rev.*, *112*(5), 1693-1701.

d'Arcy, J. A., Collins, D. J., Rowland, I. J., Padhani, A. R., & Leach, M. O. (2002). Applications of sliding window reconstruction with cartesian sampling for dynamic contrast enhanced MRI. *NMR in biomedicine*, *15*(2), 174-183.

Donoho, D. L. (2006). Compressed sensing. *Information Theory, IEEE Transactions on*, *52*(4), 1289-1306.

Griswold, M. A., Jakob, P. M., Heidemann, R. M., Nittka, M., Jellus, V., Wang, J., et al. (2002). Generalized autocalibrating partially parallel acquisitions (GRAPPA). *Magnetic Resonance in Medicine*, *47*(6), 1202-1210.

Hansen, M. S., Baltes, C., Tsao, J., Kozerke, S., Pruessmann, K. P., & Eggers, H. (2006). k-t BLAST reconstruction from non-cartesian k-t space sampling. *Magnetic Resonance in Medicine*, *55*(1), 85-91.

Hu, X., & Parrish, T. (1994). Reduction of field of view for dynamic imaging. *Magnetic Resonance in Medicine*, *31*(6), 691-694.

Huang, F., Akao, J., Vijayakumar, S., Duensing, G. R., & Limkeman, M. (2005). k-t GRAPPA: A k-space implementation for dynamic MRI with high reduction factor. *Magnetic Resonance in Medicine*, *54*(5), 1172-1184.

Irarrazabal, P., & Nishimura, D. G. (1995). Fast three dimensional magnetic resonance imaging. *Magnetic Resonance in Medicine*, *33*(5), 656-662.

Irarrazaval, P., Boubertakh, R., Razavi, R., & Hill, D. (2005). Dynamic three-dimensional undersampled data reconstruction employing temporal registration. *Magnetic Resonance in Medicine*, *54*(5), 1207-1215.

Jones, R. A., Haraldseth, O., Mller, T. B., Rinck, P. A., & Oksendal, A. N. (1993). K-space substitution: A novel dynamic imaging technique. *Magnetic Resonance in Medicine*, *29*(6), 830-834.

Jung, H., Ye, J. C., & Kim, E. Y. (2007). Improved k-t BLAST and k-t SENSE using FOCUSS. *Physics in Medicine and Biology*(11), 3201.

Kellman, P., Epstein, F. H., & McVeigh, E. R. (2001). Adaptive sensitivity encoding incorporating temporal filtering (TSENSE). *Magnetic Resonance in Medicine*, *45*(5), 846-852.

Lauterbur, P. C. (1973, 03/16). Image formation by induced local interactions: Examples employing nuclear magnetic resonance. *Nature*, *242*(5394), 190-191. (M3: 10.1038/242190a0; 10.1038/242190a0)

Lustig, M., Donoho, D., & Pauly, J. M. (2007). Sparse MRI: The application of compressed sensing for rapid MR imaging. *Magnetic Resonance in Medicine*, *58*(6), 1182-1195.

Madore, B. (2004). UNFOLD-SENSE: A parallel MRI method with self-calibration and artifact suppression. *Magnetic Resonance in Medicine*, *52*(2), 310-320.

Madore, B., Glover, G. H., & Pelc, N. J. (1999). Unaliasing by fourier-encoding the overlaps using the temporal dimension (UNFOLD), applied to cardiac imaging and fMRI. *Magnetic Resonance in Medicine*, *42*(5), 813-828.

Mistretta, C. A., Wieben, O., Velikina, J., Block, W. F., Perry, J., Wu, Y., et al. (2006). Highly constrained backprojection for time-resolved MRI. *Magnetic Resonance in Medicine*, *55*(1), 30-40.

Prieto, C., Batchelor, P. G., Hill, D. L. G., Hajnal, J. V., Guarini, M., & Irarrazaval, P. (2007). Reconstruction of undersampled dynamic images by modeling the motion of object elements. *Magnetic Resonance in Medicine*, *57*(5), 939-949.

Pruessmann, K. P., Weiger, M., Scheidegger, M. B., & Boesiger, P. (1999). SENSE: sensitivity encoding for fast MRI. *Magnetic Resonance in Medicine*, *42*(5), 952-962.

Purcell, E. M., Torrey, H. C., & Pound, R. V. (1946, Jan). Resonance absorption by nuclear magnetic moments in a solid. *Phys.Rev.*, *69*(1-2), 37-38.

Sodickson, D. K., & Manning, W. J. (1997). Simultaneous acquisition of spatial harmonics (SMASH): Fast imaging with radiofrequency coil arrays. *Magnetic Resonance in Medicine*, *38*(4), 591-603.

Stehling, M. K., Turner, R., & Mansfield, P. (1991, October 4). Echo-planar imaging: magnetic resonance imaging in a fraction of a second. *Science*, *254*(5028), 43-50.

Thedens, D. R., Irarrazaval, P., Sachs, T. S., Meyer, C. H., & Nishimura, D. G. (1999). Fast magnetic resonance coronary angiography with a three-dimensional stack of spirals trajectory. *Magnetic Resonance in Medicine*, *41*(6), 1170-1179.

Tsao, J., Boesiger, P., & Pruessmann, K. P. (2003). k-t BLAST and k-t SENSE: Dynamic MRI with high frame rate exploiting spatiotemporal correlations. *Magnetic Resonance in Medicine*, *50*(5), 1031-1042.

Vaals, J. J. V., Brummer, M. E., Dixon, W. T., Tuithof, H. H., Engels, H., Nelson, R. C., et al. (1993). ”keyhole” method for accelerating imaging of contrast agent uptake. *Journal of Magnetic Resonance Imaging*, *3*, 671-675.

Ye, J. C., Tak, S., Han, Y., & Park, H. W. (2007). Projection reconstruction MR imaging using FOCUSS. *Magnetic Resonance in Medicine*, *57*(4), 764-775.